

Chaotic Behavior of a One-dimensional Model Atom in an Intense Field *

Liu Jie ^{1,2}, Chen Shi-Gang ¹ and Bambi Hu ^{2,3}

1. Institute of Applied Physics and Computational Mathematics,
100088 Beijing, China

2. Department of Physics and Centre for Nonlinear and Complex Systems,
Hong Kong Baptist University, Hong Kong

3. Department of Physics, University of Houston, Houston, TX 77204 USA

(Received 4 July 1997)

In this paper we describe the rescattering process in optical field ionization through a one-dimensional model, which improves the well-known quasistatic model by adding the smoothed Coulomb potential in its second step. The above-threshold ionization spectra and high-order harmonic generation are calculated from this model. They are qualitatively in agreement with the quantum results and experiments. In particular, we find that this model is characterized by chaotic scattering. Modern nonlinear theory is used to analyze this dynamical system. It is found that singular self-similar fractal structure exists in the phase-dependence energy spectra, and the unstable manifolds constitute the chaotic scattering pattern. Our results also demonstrate a close connection of irregular trajectories with the energy spectra and high-order harmonic generation. We conclude that the chaotic behavior plays an important role in this one-dimensional model of optical field ionization.

PACC:

*This work was supported in part by the National Natural Science Foundation of China/19674011, the Science Foundation of the CAEP, National High Technology Committee of Laser and the Hong Kong Baptist University Faculty Research Grant.

I. INTRODUCTION

In recent years there have been significant advances in high-intensity laser technology. One major use of these laser systems has been for studies of the response of atoms and molecules to such intense fields. It has led to the discovery of a whole range of nonperturbative phenomena, such as, multiphoton ionization (MTI), above-threshold ionization (ATI), and high-order harmonic generation (HOHG). Because the fields are very intense, the traditional perturbation expansion of the wave function in terms of the field-free states will fail completely to describe the dynamics of the system. Therefore, these problems are challenging theoretically and have recently received much attention both experimentally and theoretically.^[1,2]

It has been concluded by numerical calculation of the one-electron Schrodinger equation that these phenomena can be understood in the context of single-electron ionization dynamics. Various nonperturbative theories are developed to explain ATI and HOHG phenomena. Among these theories the quasi-static model is commonly used in treatment of the optical field ionization (OFI) problem in the regime of low field frequency.^[3,4] In this model, an electron can be considered to acquire its energy in a two-step process: first the electron is removed from the atom, thereby overcoming the ionization potential, and then it interacts with the laser field. The ionization probability of the atom in the first step is usually described by the tunneling theory. Since it is in the continuum state, the evolution of an electron wave packet after tunneling is usually described by classical motions governed only by the laser field. This simple two-step quasi-classical model accounts for many of the detailed characteristics of the photon and electron emission process and provides significant insights into the excitation dynamics under intense field conditions.

However, in the case of an intense linearly polarized laser, the amplitude of the quiver motion of an electron after tunneling is large. Then the probability that an ionized electron returns to the vicinity of the nucleus and is rescattered by the ion is not negligible. This problem attracts much attention and becomes an active point recently. Many classical and quantum theories are developed to treat this rescattering process.^[5,6,7] It is found that this process may increase the fraction of the electron with higher energy, and is responsible for other important phenomena, such as the 'cut off' law in high-order harmonic generation. Different from the above works, in this paper we try to consider the rescattering process in the frame of one-dimensional (1D) quasiclassical model, which is derived from natural extending of the original quasistatic model by adding a smoothed Coulomb potential in its acceleration step. In sec.II we will introduce this 1D model. According to this model the above-threshold energy spectra and high-order harmonic generation in the rescattering process are calculated in sec.V. Our results show that the rescattering process increases the higher energy electron and generates high-order harmonics. Additionally, the 'cut off' law is identified by this model. In particular, based on nonlinear theories, we discover a new physical process - chaotic scattering underlying optical field ionization and give a complete dynamical explanation for them (secs.III and IV). We find that self-similar and fractal structure exists in the plots of ATI energy vs initial field phase. We also identify those unresolved regions of ATI energy with chaotic layers. The location and width of those singular regions are estimated by a nonlinear theory. In sec.VI we analyze the dynamical structure in Poincare section which causes the chaotic scattering. Finally in sec.VII we

summarize our main results and discuss some problems for future study.

II. THE MODEL

First let us recall the well-known quasistatic theory briefly. As $\gamma \equiv (I_0/2U_p)^{1/2} \ll 1$, $\hbar\omega/2U_p \ll 1$ and field strength $F < F_{th} \equiv Z^3/16n_{eff}^4 a.u.$ (atomic units are used in this paper), tunneling ionization occurs. Here, I_0 is the ionization potential of the electron, $U_p = \frac{Z^2 e^2 F^2}{4m_e \omega^2}$ is the ponderomotive potential, F_{th} is the threshold field, Z is the core charge and n_{eff} is the effective principle quantum number. The corresponding threshold intensity of F_{th} is

$$I_{th} = 1.37 \times 10^{14} (I_0/13.6 eV)^4 / Z^2 \quad (W/cm^2). \quad (1)$$

Based on the Landau tunneling ionization theory,^[8], Ammosov, et al.^[9] suggested a simple formula for the ionization rate of complex atoms:

$$\Gamma(F) = 1.61 \frac{Z^2}{n_{eff}^{4.5}} \left(\frac{10.87 Z^3}{n_{eff}^4 F} \right)^{2n_{eff}-1.5} \exp\left(-\frac{2}{3} \frac{Z^3}{n_{eff}^3 F}\right) \quad a.u. \quad (2)$$

This formula is commonly used in estimating the ATI energy of the ionized electrons.^[10]

The second part of the quasistatic procedure uses classical mechanics to describe the evolution of an electron packet. After tunneling, the electron motion in the field is given by

$$\begin{aligned} x &= x_0[\cos(\omega t)] + v_{0x}t + x_{0x}, \\ v_x &= -v_0 \sin(\omega t) + v_{0x}, \end{aligned} \quad (3)$$

where $v_0 = ZeF/m_e \omega$, $x_0 = ZeF/m_e \omega^2$. The energy associated with the velocity v_{0x} constitutes the ATI energy and can be evaluated by averaging over the external field

$$E_{ATI} = U_p[1 + 2 \sin^2 \phi_0], \quad (4)$$

where $\phi_0 = \omega t_0$ denotes the field phase.

In a linearly polarized intense laser field, the amplitude of the quiver motion is large. Then the ionized electrons are driven by the laser field to return to the vicinity of the ions and are rescattered by them. This process will result in many important phenomena, such as 'plateau' in ATI peaks, 'ring' in angular distribution and 'cut-off' law of high-order harmonic generation. To take the rescattering process into consideration, we improve the above model by adding a smoothed Coulomb potential in its second procedure. Then the governing equation is (the atomic units is used for simplicity),

$$H = \frac{p^2}{2} - \frac{1}{\sqrt{x^2 + \alpha}} + exF \cos(\omega t), \quad (5)$$

where $\alpha = 0.1$ the 'softening' factor to normalize the Coulomb potential.

The initial position of an electron borne outside the potential barrier at time t_0 is determined by the tunneling ionization theory,

$$U_{eff} = -\frac{Ze^2}{\sqrt{x_0^2 + \alpha}} + eFx_0\cos(\omega t_0) = I_0, \quad (6)$$

where $I_0 = 0.5$ is the ionization potential.

Take $\pi/2 < \omega t_0 < 3\pi/2$ as an example. It is observed that the electron corresponding to the maximum field strength ($\omega t_0 = \pi$) is closest to the nucleus. As $\omega t_0 = \frac{\pi}{2}$ or $\frac{3\pi}{2}$, the initial electron position tends to positive infinity. Due to the fact that an electron will be in the continuum state after tunneling ionization, we prefer to choose the initial energy rather than its initial momentum of an ionized electron born at time t_0 to be zero. That is, if the external field is removed away at time t_0 the ionized electron will escape away from the Coulomb potential. On the contrary, the condition that the initial momentum is zero cannot guarantee the escaping of the ionized electron.^[11] Then the initial momentum of an ionized electron can be derived from the above assumption. These initial conditions are sufficient for us to study the rescattering effects in the following sections.

III. SELF-SIMILAR FRACTAL STRUCTURE AND SCALING LAW

It is convenient to introduce the compensated energy E_c advocated by Leopold and Percival,^[12]

$$E_c = [v_x - (F/\omega)\sin(\omega t)]^2/2 - 1/\sqrt{x^2 + \alpha}, \quad (7)$$

When an electron is ionized completely and cannot return to the nucleus again, the Coulomb potential is weak enough and E_c tends to a positive constant value which is just the ATI energy (E_{ATI}) in ultrashort pulse laser.

FIGURES

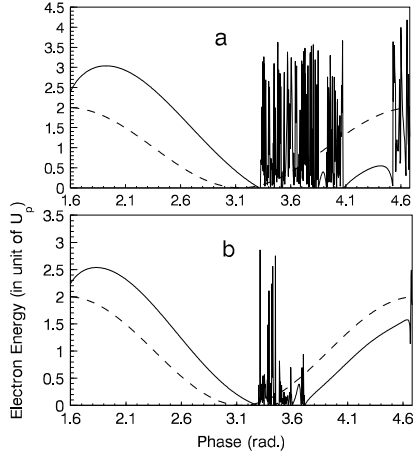


FIG. 1. Plots of electron energy vs field phase. Dashed lines and solid lines denote the results from original model and the present model respectively. a) $F = 0.06a.u.$, $\omega = 0.07a.u.$ b) $F = 0.06a.u.$, $\omega = 0.04242a.u..$

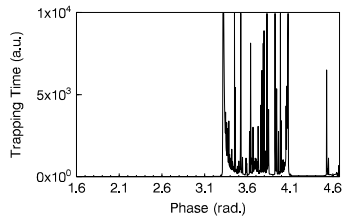


FIG. 2. Trapping time vs field phase. $F = 0.06a.u.$, $\omega = 0.04242a.u..$

In Fig.1 we demonstrate the phase dependence of the ATI energy. A Runge-Kutta algorithm of the 4th order in x and p is employed in the calculations. One thousand points distributed equally in the range $[\pi/2, 3\pi/2]$ are chosen as the initial phase. It was observed that the curves calculated from the original model where the Coulomb potential is neglected are smooth over all the range; however, in our new model things are much different. The dependence of E_{ATI} on the initial phases is poorly resolved in the region $[3.32, 4.05]$, $[4.52, 4.71]$ for $\omega = 0.07a.u.$ and in the region $[3.30, 3.70]$, $[4.69, 4.71]$ for $\omega = 0.04242a.u..$ Magnification of the unresolved regions shows that an arbitrarily small change in the initial phase may result in a large change in the final electron energy. We define the escaping time of an electron as the moment T ^[13] satisfying

$$E_c(t = T) = 0, \quad E_c(t > T) > 0. \quad (8)$$

Naturally, the trapping time of an electron is defined as $\Delta T = T - t_0$. A comparison between Fig.1 and Fig.2 shows that the unresolved regions in Fig.1 coincide with the singularities of the trapping time.

We call a value ϕ_s a singularity if, in any small neighborhood domain there is a pair of ϕ which have different signs in their final moments. These singular values relate to the infinite trapping time. Generally in phase space they constitute a nonattracting hyperbolic invariant set. This invariant set has a fractal structure. Figure 3 shows successive magnification of the unresolved region and demonstrates clearly the existence of self-similarity.

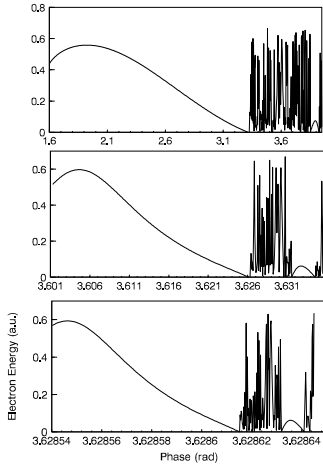


FIG. 3. Successive magnification of the plot for $F = 0.06a.u.$, $\omega = 0.07a.u..$

To calculate the fractal dimension of the singular points ϕ_s , we can employ the uncertainty exponent technique to obtain the fractal dimension of the singular set.^[14] We randomly choose many values of ϕ in an interval containing the fractal set. We then perturb each value by an amount ϵ and determine whether the final momentum corresponding to initial ϕ , $\phi - \epsilon$ and $\phi + \epsilon$ have the same sign. If so, we say that the ϕ value is ϵ -certain; if not, we say it is ϵ -uncertain. We do this for several ϵ and plot on a log-log scale the fraction of uncertain ϕ values $f(\epsilon)$. The result is plotted in Fig.4 which shows a good straight line and indicates a power law dependence $f(\epsilon) \sim \epsilon^\gamma$, where $\gamma = 0.15$. The exponent γ is related to the dimension of the fractal set of the singular ϕ values by

$$D_0 = 1 - \gamma = 0.85. \quad (9)$$

In another aspect, it is interesting to make an intensive investigation on the escaping process of an electron after tunneling. We find that the trajectories demonstrate much different behavior for different initial phase. Some electrons drifts away from nucleus without a collision, others can undergo multiple collisions. In Fig.5 we plot the probability vs. the collision times by making a statistics on 4000 trajectories corresponding to different phases. It is found that, approximately the probability decays with increasing collision times and satisfies the following scaling law

$$P_{col} \sim e^{-\kappa N}, \quad (10)$$

where $\kappa = 0.21$, N denotes the collision number.

Obviously, the possibility of multiple collisions decreases exponentially with increasing collision number. Although chaos implies the existence of infinite times of collisions, its probability is zero. This is because the hyperbolic invariant set corresponding to the trapped trajectories has zero measure.

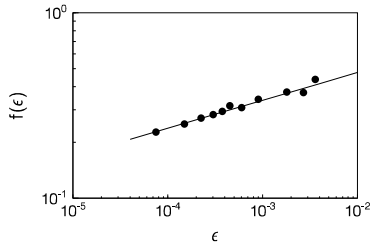


FIG. 4. Calculation of fractal dimension in the case $F = 0.06a.u.$, $\omega = 0.07a.u.$

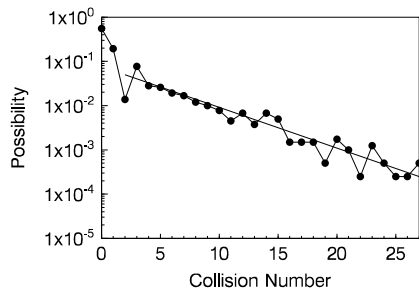


FIG. 5. Probability of multiple collisions obtained from making statistics on 4000 trajectories corresponding to different initial phase (circle). The straight line denotes the scaling law mentioned in the text.

IV. UNRESOLVED REGIONS RESULTING FROM CHAOTIC LAYERS

In previous sections we discovered that the unresolved regions have an irregular, self-similar fractal structure. In this section we will discuss the dynamical source of these phe-

nomena. We will determine the location and width of the unresolved regions by using modern nonlinear theory.

First let us review some important conclusions ^[15] on a two-dimensional (2D) area-preserving mapping described by

$$\bar{E} = E + \Delta E, \quad \bar{\phi} = \phi + f(\bar{E}) \quad (11)$$

In the neighborhood of a separatrix (E_s), where the period $f(E_s)$ tends to infinity, even small changes in energy E may result in considerable changes in phase ϕ . This is the very cause of local stochasticity. The following expression can be served as a good evaluation of the stochastic region boundary

$$\left| \frac{\delta \bar{\phi}}{\delta \phi} - 1 \right| > \pi. \quad (12)$$

In the rest of this section we shall employ the Kramers-Hennerberger (or acceleration) gauge and atomic units will be used to simplify our formula. The variable transformations are

$$P = p + \frac{\epsilon}{\omega} \sin \omega t, \quad X = x - \frac{\epsilon}{\omega^2} \cos \omega t. \quad (13)$$

The new Hamiltonian is

$$K(X, P) = \frac{P^2}{2} - \frac{1}{\sqrt{(X + \frac{\epsilon}{\omega^2} \cos \omega t)^2 + \alpha}}. \quad (14)$$

The corresponding equations of motion are

$$\dot{X} = P, \quad \dot{P} = -\frac{X + \frac{\epsilon}{\omega^2} \cos \omega t}{(X + \frac{\epsilon}{\omega^2} \cos \omega t)^2 + \alpha}^{\frac{3}{2}}. \quad (15)$$

The fundamental property of the Hamiltonian system is that the Cartan differential 2-form

$$dP \wedge dX - dH \wedge dt \quad (16)$$

is preserved under Hamiltonian flow. As the term $\frac{\epsilon}{\omega^2} \cos \omega t$ in (16) vanishes, the energy

$$E_0 = \frac{P^2}{2} - \frac{1}{\sqrt{X^2 + \alpha}}. \quad (17)$$

is an integral constant. Otherwise, its evolution is time-dependent and can be described approximately by virtue of Eqs. (16) and (18)

$$\frac{dE_0}{dt} = \frac{2\epsilon}{\omega^2} P X \cos \omega t / (X^2 + \alpha)^2. \quad (18)$$

To evaluate the jump in energy, we consider the following straight-line trajectory as the zeroth-order approximation,

$$P = v_c, \quad X = v_c(t - \tau), \quad (19)$$

where v_c and τ are the momentum and time, respectively, at $X = 0$. Then the jump of the energy for each return is obtained by integrating Eq.(19) from negative infinity to positive infinity,

$$\Delta E_0 = \frac{2\epsilon}{\omega^2} \int_{-\infty}^{+\infty} v_c^2(t - \tau) \cos \omega t / (v_c^2(t - \tau)^2 + \alpha)^2 dt. \quad (20)$$

The above integral can be rewritten in a simpler form,

$$\Delta E_0 = \frac{\epsilon}{v_c^2} \sin \omega \tau \int_{-\infty}^{+\infty} \frac{\cos(s)}{s^2 + \alpha \omega^2 / v_c^2} ds, \quad (21)$$

The integral included in the above formula can be expressed in term of a Bessel function,

$$K_{\frac{1}{2}}(z) = \frac{(2z)^{\frac{1}{2}}}{2\sqrt{\pi}} \int_{-\infty}^{+\infty} \frac{\cos t}{(t^2 + z^2)} dt, \quad (22)$$

where $z = \alpha^{\frac{1}{2}} \omega / v_c$. Now we divide our problem into the following two cases.

A. Case 1, $E_{s1} = 0$. The jump of energy is rewritten as

$$\Delta E_0 = \delta E_{s1} \sin \phi, \quad \phi = \omega \tau, \quad (23)$$

where

$$\delta E_{s1} = \frac{\epsilon}{v_{c1}^2} \int_{-\infty}^{+\infty} \frac{\cos(s)}{s^2 + \alpha \omega^2 / v_{c1}^2} ds. \quad (24)$$

and v_{c1} is derived from Eq.(18) by setting $E_0 = E_{s1}$ and $X = 0$. As the 'softening' factor α is usually chosen as a small value, the Keplerian Law of the two-body problem is available approximately. Therefore, we obtain the corresponding change of phase as follows,

$$\bar{\phi} = \phi + \frac{\omega \pi}{|E_0|^{\frac{3}{2}}}. \quad (25)$$

Equations (24) and (26) construct a 2D mapping which reflects the dynamical properties of the system (15) in the vicinity of $E = E_{s1}$. The area-preserving nature of this mapping, a consequence of the invariance of the Cartan differential 2-form (17), can be checked easily.

In terms of the nonlinear theory mentioned at the beginning of this section, we conclude that there exists a chaotic layer in the vicinity of $E = E_{s1}$, the width of it is determined by condition (13). Then we get

$$0 < E_{s1} - E_0 < \left(\frac{3}{2}\omega \delta E_{s1}\right)^{\frac{2}{5}}. \quad (26)$$

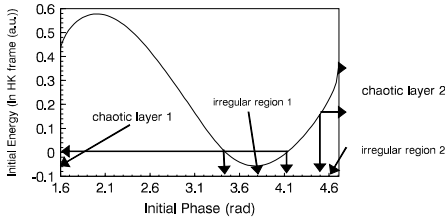


FIG. 6. The chaotic layers predicted theoretically, showing coincidence with those unresolved regions. $F = 0.06a.u.$, $\omega = 0.07a.u.$

In Fig.6 we plot the initial energy vs the initial field phase. The above inequality determines a chaotic layer. We find that this chaotic layer coincides with the larger one of the two unresolved regions in Fig.1.

B. Case 2, $E_{s2} = \frac{\epsilon^2}{2\omega^2}$. The jump of energy can also be rewritten in the same form as in Eqs.(24) and (25) . The v_{c2} is derived from Eq.(18) by assuming that $E_0 = E_{s2}$, $X = 0$.

The change of phase is derived by evaluating the following integral,

$$\bar{\phi} = \phi + \omega \int_0^{x_0} dx / \sqrt{2E_0 + 2/(x^2 + \alpha)^{\frac{1}{2}}}, \quad (27)$$

where x_0 is the initial position which is given by Eq.(7). As $E_0 \rightarrow E_{s2}$, $X_0 \rightarrow \infty$ and the following approximation is applicable,

$$X_0 \simeq -1/2F \cos \omega t_0, \quad E_0 \simeq \frac{\epsilon^2}{2\omega^2} + 2F \cos \omega t_0. \quad (28)$$

Then we obtain approximately $X_0 \simeq \frac{1}{E_0 - E_{s2}}$. As $E_0 \rightarrow E_{s2}$, we approximate Eq.(28) by

$$\bar{\phi} = \phi + \frac{1}{\sqrt{2E_{s2}}} \frac{\omega}{E_{s2} - E_0}. \quad (29)$$

Similar discussions as in case 1 can be done. We obtain the following expression which determines a chaotic layer,

$$0 < E_{s2} - E_0 < \left(\frac{\omega \delta E_{s2}}{\pi \sqrt{2E_{s2}}} \right)^{\frac{1}{2}}. \quad (30)$$

Figure 6 shows that this chaotic layer coincides with the smaller one of the two unresolved regions in Fig.1. Actually, in case 2, the change of energy δE_{s2} for the first collision is large enough . This fact makes it possible that these points will fall into irregular region one finally. That is, in the Poincare section, the two chaotic layers expressed by Eqs. (27) and (31) respectively are located in the same connected region.

V. ATI SPECTRA AND HOHG IN THE RESCATTERING PROCESS

Because the amplitude of the field varies slowly with time in the tunneling regime , the phase dependence of the ionization rate can be expressed as follows^[8],

$$\Gamma(\phi) = \frac{4}{3} \exp\left(-\frac{2}{3|\epsilon \cos \phi|}\right) \text{ a.u..} \quad (31)$$

In terms of the original model in which the Coulomb potential and rescattering are neglected, the ATI energy of an ionized electron in linearly polarized laser beams takes the form

$$E_{ATI}(\phi) = 2U_p \sin^2 \phi. \quad (32)$$

Then the energy distribution of the ionized electrons is evaluated by the following expression,

$$P(E_{ATI})dE_{ATI} = \Gamma(\phi)d\phi, \quad P(E_{ATI}) = \Gamma(\phi) \frac{d\phi}{dE_{ATI}}. \quad (33)$$

The plots of the distribution of electron energy are shown in Fig.7, which represents a steeply decreasing curve. Some ionization experiments are performed in the tunneling regime to test and verify the quasi-static theory. Analysis shows that qualitatively the prediction of the two-step theory agrees with the experimental data, and it gives a much smaller fraction of the high-energy ionized electrons.^[1]

In terms of the improved model, because of the rescattering effects, the final energy of the detected electrons in a short pulse experiment can be larger than $2U_p$. The initial phase may be divided into four different regions: [1.57,3.32], [3.32,4.05],[4.05,4.52] and [4.52,4.71] for $\omega = 0.07 \text{ a.u.}$, $\epsilon = 0.06 \text{ a.u.}$, and [1.57,3.30], [3.30,3.70],[3.70,4.69] and [4.69,4.71] for $\omega = 0.04242 \text{ a.u.}$, $\epsilon = 0.06 \text{ a.u.}$. The trajectories initiating in different regions show quite different behaviors (Fig.8). The electrons starting from the first region drift away from the nucleus without a collision. Those electrons originating from the third region must recross the original point once before completely escaping. However, the electrons initiating in regions 2 and 4 can undergo multiple collisions with the nucleus and absorb more photons in this rescattering process. As was mentioned above, the trajectories starting from regions 1 and region 3 are regular, and from regions 2 and 4 may be irregular. In the situation that the initial phase is in region 4, the tunneling barrier is too broad for any significant release to occur. Then the effects of chaotic rescattering in region 2 may influence strongly the final energy distribution.

Because of chaotic rescattering the function E_{ATI} is not differentiable almost everywhere in those irregular regions . The usual Riemann integral can not be applied to obtain the energy distribution, and the Lebesgue integral is introduced to deal with the problem. The probability of the kinetic energy of electrons falling into the interval $[E, E + \Delta E]$ is

$$P = \text{Les.} \int_S E_{ATI}(\phi) \Gamma(\phi) d\phi, \quad (34)$$

where S denotes a set of initial phase ϕ satisfying $E < E_{ATI}(\phi) < E + \Delta E$, $\Delta E = U_p/10$.

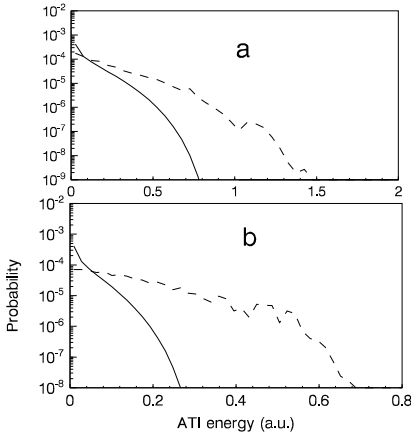


FIG. 7. Energy spectra for *a*) $F = 0.06$ a.u., $\omega = 0.04242$ a.u. *b*) $F = 0.06$ a.u., $\omega = 0.07$ a.u.. The solid lines and dotted lines denote the results from the original model and the present model respectively.

In Fig.7 we plot the energy distribution according to the above formula. It shows clearly that rescattering increases the fraction of the electrons with higher energy. This is because the electrons which have more probability of staying in the vicinity of the nucleus will absorb more photons. This result is also qualitatively in agreement with that of our quantum approaches [8]. In numerical simulations, 1000 initial trajectories are used. We also calculate the ATI spectra by using 10000 trajectories. We find that they are agreeable except for a little fluctuation in the higher energy range.

Another consequence of the electron-ion interaction is emission of light. The emission can be calculated from the expectation value of the dipole operator

$$d(t) = \langle \psi | ex | \psi \rangle, \quad (35)$$

where ψ is the Floquet state.

In terms of the symmetry of the Hamiltonian $H_0(x, p) = H_0(-x, -p)$ and the periodicity of the external field, Floquet theorem guarantees that the Fourier decomposition of $d(t)$ contains neither even nor constant harmonic but odd harmonics dipole component.^[16]

After tunneling the density of states available to electron is large enough so that its subsequent evolution should be accurately characterized by classical motion. Then the spectral analysis of the classical trajectories can reveal the mechanism responsible for high-order harmonic generation in the rescattering process. We consider the power spectrum or spectral density of the dipole moment function $x(t)$ in the classical case,

$$I(\omega) = (1/2\pi) \lim_{T \rightarrow \infty} (1/2T) \langle \left| \int_0^{2T} ex(t) \exp(-i\omega t) dt \right|^2 \rangle, \quad (36)$$

where $\langle \rangle$ indicates an average over field phases ϕ .

Actually analysis of a single trajectory is sufficient to illustrate the underlying mechanisms.^[17,18] Four types of classical trajectory related to rescattering are shown in Fig.8. For regular trajectories (types 1 and 3) the power spectrum consists of only a single

peak precisely located at the laser frequency because Rayleigh scattering is dominant in this case. Things are much different for trajectories originating from in regions 2 and 4. Figure 9 shows the dipole moment function and its corresponding power spectrum for a trajectory initiated in the irregular regions. In this case, the electron is first pumped by the external fields far away from the nucleus for a long time before returning to the ion and emits light. Only when the electron is close to the nucleus, can the electron exchange energy efficiently with the electromagnetic field. After oscillating around the nucleus for about 10 optical cycles, the electron absorbs more photons and is ejected to the continuum. A power spectrum analysis of the dipole moment is made in the time interval [10000, 11000] when the electron oscillates near the nucleus. The power spectrum shows that high harmonics up to 33rd are generated in the process. The magnitude of the peaks decreases monotonically approximately with increasing order. The peak corresponding to 33rd harmonic is about three orders lower than that of Rayleigh scattering. The even harmonics component appearing in the power spectrum can be removed by averaging over an ensemble of classical trajectories.

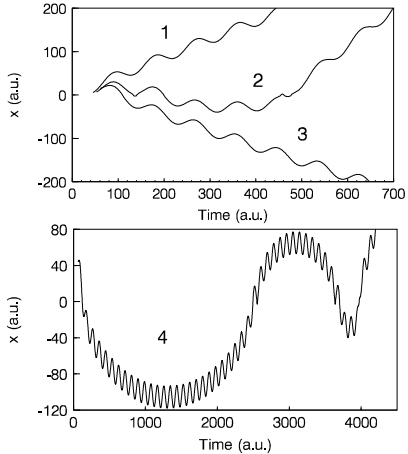


FIG. 8. Typical trajectories initiated in four different regions.

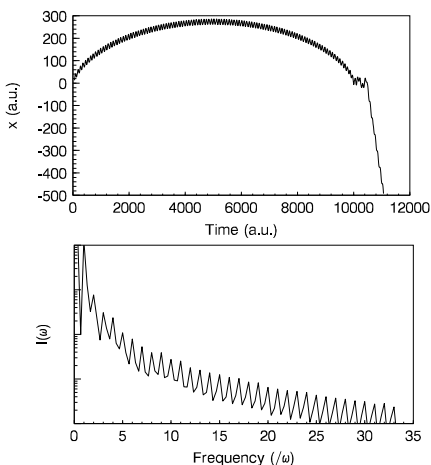


FIG. 9. The dipole moment as a function of time and corresponding power spectrum for a typical trajectory initiated in irregular regions. $\phi_0 = 3.3250968504$, $F = 0.06a.u.$, $\omega = 0.07a.u..$

In the high-intensity regime a new contribution to harmonic emission becomes possible. That is, while an electron is near the nucleus it can make a transition back to the ground state, emitting a high-energy photon. Obviously the energy of the resulting photon corresponds to the energy (return energy E_r) the electron has when it collides with the core. This return energy depends strongly on the field phase at which the electron escapes through the potential barrier. In Figs.10(a) and 11(a) we plot the return energy vs the phase for $\omega = 0.04242a.u.$ and $\omega = 0.021a.u.$ respectively. The 1000 initial phases distributed equally in the interval $[\pi/2, 3\pi/2]$ are used in the calculation. In Figs.10(b) and 11(b) we show the histograms of the return energies weighted by the tunneling rate appropriate to the initial conditions for each trajectory. The result is a broad, flat distribution followed by an abrupt cutoff. The sharp cutoff in the electron energy occurs at $3.5U_p$ for $\omega = 0.04242a.u.$ and at $3.3U_p$ for $\omega = 0.021a.u.$ respectively. We think this is the physical origin of the cutoff law for high harmonic radiation.^[6,19] The smaller the field frequency, the more the tunneling condition is satisfied. Therefore the value of the cutoff energy tends to $3.2U_p$, which has been supported by experimental evidence.

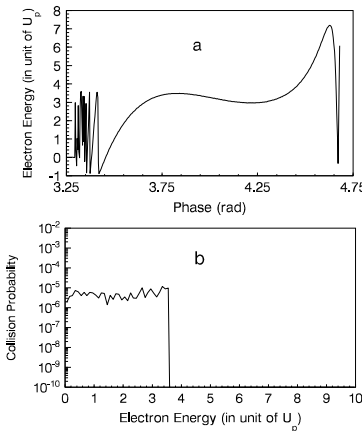


FIG. 10. a) The energy of returning electron as a function of field phase. b) Energy histogram for electron trajectories returning to the nucleus. $\omega = 0.04242a.u.$ and $F = 0.06a.u..$

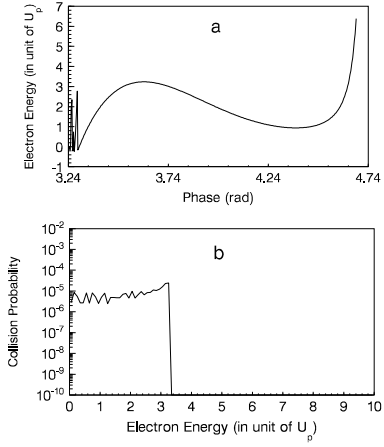


FIG. 11. a) The energy of returning electron as a function of field phase. b) Energy histogram for electron trajectories returning to the nucleus. $\omega = 0.021a.u.$ and $F = 0.06a.u..$

VI. DYNAMICAL STRUCTURE IN POINCARE SECTION

Irregular behavior of the electrons in the rescattering process is characterized by the singularity of the final ATI energy distribution. This singularity is attributed to chaotic scattering in system (15). The system studied in previous sections constitutes an excellent physical system for the investigation of chaotic scattering. The physical process that we have in mind involves the rescattering in the OFI problem.

To study chaotic scattering, we choose the initial condition as the points in phase space well in the asymptotic region of the potential, typically, $X = 100 a.u.$ and P in the range $[0, -1.5] a.u..$ Figure 12 shows the stroboscopic map, $(X(t), P(t))|_{\omega t=0} (mod 2\pi)$, for such an ensemble of 200 scattering trajectories. Further the system can flow arbitrarily between the bounded and unbounded regimes, so it is a non-compact system. The phase section shows a rich and complicated structure. As the system is periodically perturbed, the Poincare section is naturally defined as $\sum : \omega t = 2k\pi$. The corresponding Poincare mapping is expressed as

$$M : (X', P') = M \circ (X, P) = (F(X, P), G(X, P)), \quad (37)$$

where (X', P') is the point at $\omega t = \omega t_0 + 2\pi$ of the trajectory initiating in (X, P) at ωt_0 . Its corresponding tangent mapping will be

$$TM : (\delta X', \delta P') = \left(\frac{\partial F}{\partial X} \delta X + \frac{\partial F}{\partial P} \delta P, \frac{\partial G}{\partial X} \delta X + \frac{\partial G}{\partial P} \delta P \right). \quad (38)$$

In the following discussions t_0 is set to be zero without losing generality.

The variational equations of the Hamiltonian system are

$$\begin{aligned} \frac{d(\delta X)}{dt} &= \frac{\partial^2 K}{\partial P \partial X} \delta X + \frac{\partial^2 K}{\partial P \partial P} \delta P, \\ \frac{d(\delta P)}{dt} &= -\frac{\partial^2 K}{\partial X \partial X} \delta X - \frac{\partial^2 K}{\partial X \partial P} \delta P. \end{aligned} \quad (39)$$

Equations (16) and (40) constitute a four-dimensional non-autonomous dynamical system. Tracing the trajectories initiating in $(X_0, P_0, 1, 0), t_0 = 0$ and $(X_0, P_0, 0, 1), t_0 = 0$ by using a 4th order Runge-Kutta algorithm in x and p , we can get the solutions $(X_1, P_1, \delta X_1, \delta P_1)$ and $(X_1, P_1, \delta X_2, \delta P_2)$ at time $\omega t = 2\pi$ respectively. The Poincare mapping and its tangent mapping can be calculated numerically according to following expressions:

$$X_1 = F(X_0, P_0), P_1 = G(X_0, P_0), \quad (40)$$

$$\frac{\partial X_1}{\partial X_0} = \frac{\partial F}{\partial X_0} = \delta X_1, \quad (41)$$

$$\frac{\partial P_1}{\partial X_0} = \frac{\partial G}{\partial X_0} = \delta P_1.$$

$$\frac{\partial X_1}{\partial P_0} = \frac{\partial F}{\partial P_0} = \delta X_2, \quad (42)$$

$$\frac{\partial P_1}{\partial P_0} = \frac{\partial G}{\partial P_0} = \delta P_2.$$

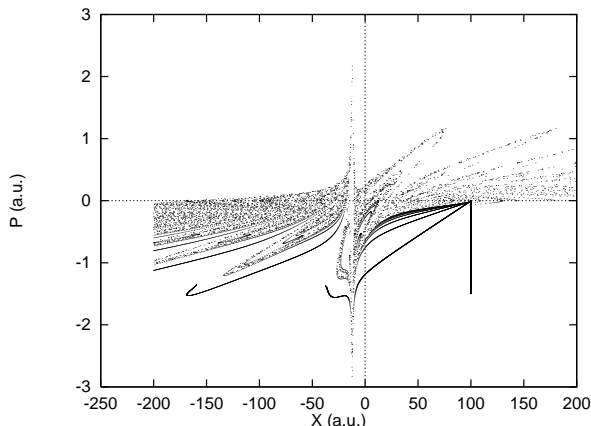


FIG. 12. Stroboscopic map for 200 trajectories originating asymptotically at $X = 100$ with P in range $[0, -1.5]$. $F = 0.06$ a.u., $\omega = 0.07$ a.u..

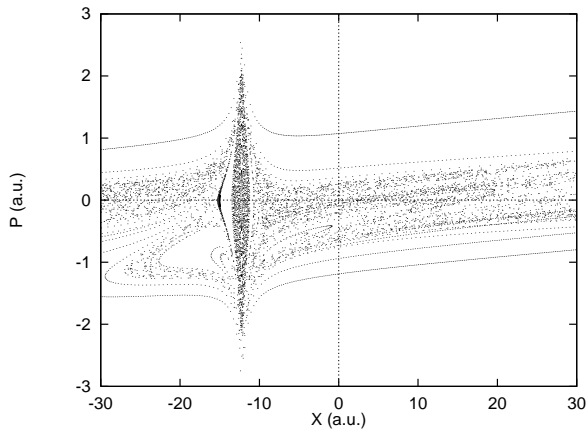


FIG. 13. Phase plane of Poincare mapping M for $F = 0.06$ a.u., $\omega = 0.07$ a.u..

Since the Cartan differential 2-form is conserved under Hamiltonian flow, the mapping M should conserve $dX \wedge dP$, that is, it is area-preserving. Because of the symmetry of the Hamiltonian system, the 1-periodic fixed points are located on the X -axis. The Newton-Raphson algorithm is employed to locate these fixed points precisely. They are $P_1(-15.95186600603247, 0)$, $P_2(-15.02, 0)$, $P_3(-12.25, 0)$, $P_4(-9.30, 0)$, $P_5(2.80, 0)$, $P_6(15.87, 0)$. P_2 and P_3 are stable elliptic fixed points, others are unstable hyperbolic fixed points. Figure 13 shows the phase plane of the mapping M . Around P_3 there is a larger stable region where KAM curves exist. The stable region around P_2 is too small to be distinguished in the plots.

From the symmetry $K(X, -P, -t) = K(X, P, t)$, the stable manifolds and unstable manifolds are symmetric about the X -axis. In Fig.14 we plot the unstable manifolds of these four hyperbolic fixed points by using the method suggested in Ref.[21]. Clearly, they intersect the X -axis. So we conclude that the unstable manifolds and stable manifolds intersect each other transversely. The intersection points constitute a hyperbolic invariant set with a fractal dimension which has been mentioned in section III. The Smale structure occurs in the phase plane. This is the dynamical source of chaotic scattering. Comparing Figs.12, 13 and 14, we find that the unstable manifolds organize the scattering pattern and the phase plane structure.

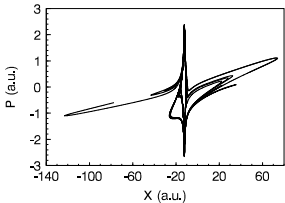


FIG. 14. The unstable manifolds of period-1 saddles of mapping M for $F = 0.06a.u.$, $\omega = 0.07a.u.$

VII. DISCUSSIONS AND CONCLUSIONS

Recent advances in classical nonlinear dynamics and chaos have had important applications in the description of the photoabsorption spectrum of Rydberg atoms in strong magnetic fields,^[22] and the microwave ionization of highly excited hydrogen atoms.^[23] These discussions extremely enrich the atomic physics. More recently, some pioneer nonlinear dynamicist begin to deal with the topics of atoms in intense fields. Sundaram and Jensen^[24] connect the ionization suppression with 'scarred' wave functions. Benvenuto *et al.*^[25] estimate the parameter regime of atom stabilization according to the border of chaos. Cocke and

Reichl^[26] calculate the HONG in the frame of 1D model atom and conclude that it implies chaos. Richards^[27] has studied 1D excited hydrogen atoms in short-pulsed high-frequency fields and find the signs of incipient chaos. The purpose of this paper is to apply the nonlinear theory in ATI and HOHG according to a 1D description of optical field ionization in the regime of low field frequency. We discover a new physical process - chaotic scattering underlying the optical field ionization process. Modern nonlinear theory is applied to analyze the chaotic behavior of this nonlinear system. Chaotic layers and self-similar fractal structure are found in this model. Otherwise we find that unstable and stable manifolds organize the chaotic scattering pattern.

In another aspect, the above-threshold ionization energy spectra and high-order harmonic generation are discussed according to the improved quasi-static model. The rescattering effects on ATI spectra and high-order harmonic generation are discussed. The result that rescattering increases the fraction of the electrons with higher energy is qualitatively in agreement with our previous works from a quantum approach. The cutoff law for high harmonic radiation is identified by our new model. In particular, We have shown the connection between regular and irregular trajectories and ATI , HOHG phenomena. We find that chaotic behavior plays an important role in these processes.

In this paper, our discussions are restricted to 1D model . A question that can not be evaded is: Whether the above discussions are helpful to the understanding of the ionization process of a real atom in a three-dimensional (3D) space ? The Key point of this problem is whether multiple collisions (resulting in chaos) still occur in a 3D case. It seems that there are only trivial number of multiple return trajectories. Actually, this is a specious argument. In our 3D extension of the above model, numerical simulations show that there do exist a number of (not trivial number) trajectories which return to the core more than once and those multiple collisions trajectories (chaos) play an important role in energy spectra and angular distribution of the final hot electrons (results in details will be reported elsewhere) . Therefore, we believe that our discussions on 1D model is much helpful to the understanding of the ionization process of a real atom in a 3D case.

Notes: After we completed this manuscript, we find that the authors of Ref. [28] have made some researches on the effects of multiple returns on double ionization for 3D model, and show an enhancement by more than an order of magnitude.

CAPTIONS OF FIGURES

- Fig.1 Plots of electron energy vs field phase. Dashed lines and solid lines denote the results from original model and the present model respectively. a) $F = 0.06a.u.$, $\omega = 0.07a.u.$ b) $F = 0.06a.u.$, $\omega = 0.04242a.u..$
- Fig.2 Trapping time vs field phase. $F = 0.06a.u.$, $\omega = 0.04242a.u..$
- Fig.3 Successive magnification of the plot for $F = 0.06a.u.$, $\omega = 0.07a.u..$
- Fig.4 Calculation of fractal dimension in the case $F = 0.06a.u.$, $\omega = 0.07a.u..$
- Fig.5 Probability of multiple collisions obtained from making statistics on 4000 trajectories corresponding to different initial phase (circle). The straight line denotes the scaling law mentioned in the text.
- Fig.6 The chaotic layers predicted theoretically, showing coincidence with those unresolved regions. $F = 0.06a.u.$, $\omega = 0.07a.u..$
- Fig.7 Energy spectra for a) $F = 0.06a.u.$, $\omega = 0.04242a.u.$ b) $F = 0.06a.u.$, $\omega = 0.07a.u..$ The solid lines and dotted lines denote the results from the original model and the present model respectively.
- Fig.8 Typical trajectories initiated in four different regions.
- Fig.9 The dipole moment as a function of time and corresponding power spectrum for a typical trajectory initiated in irregular regions. $\phi_0 = 3.3250968504$, $F = 0.06a.u.$, $\omega = 0.07a.u..$
- Fig.10 a) The energy of returning electron as a function of field phase. b) Energy histogram for electron trajectories returning to the nucleus. $\omega = 0.04242a.u..$ and $F = 0.06a.u..$
- Fig.11 a) The energy of returning electron as a function of field phase. b) Energy histogram for electron trajectories returning to the nucleus. $\omega = 0.021a.u..$ and $F = 0.06a.u..$
- Fig.12 Stroboscopic map for 200 trajectories originating asymptotically at $X = 100$ with P in range $[0, -1.5]$. $F = 0.06a.u.$, $\omega = 0.07a.u..$
- Fig.13 Phase plane of Poincare mapping M for $F = 0.06a.u.$, $\omega = 0.07a.u..$
- Fig.14 The unstable manifolds of period-1 saddles of mapping M for $F = 0.06a.u.$, $\omega = 0.07a.u..$

REFERENCES

- [1] 'Atoms in Intense Laser Fields', Ed. M.Gavrila, Academic Press, INC. (1992)
- [2] 'Super-Intense Laser-Atom Physics', Ed. Bernard Piraux, Anne L'Huillier and Kazimierz Rzazeewski, Plenum Press, New York, (1993)
- [3] P.B.Corkum, Phys. Rev. Lett. **71**, (1993) 1994
- [4] J.L.Krause, K.J.Schafer and K.C.Kulander, Phys.Rev.Lett. **68**, (1992), 3535
- [5] G.G.Paulus, W.Nicklich, Huale Xu, P.Lambropoulos and H.Walther, Phys. Rev. Lett. **72**, (1994), 2851 G.G.Paulus, W.Becker, W.Nicklich and H.Walther, J.Phys.B:At.Mol.Opt.Phys. **27** (1994) L703
- [6] W.Becker, A.Lohr, M.Kleber, J.Phys.B: At.Mol.Opt.Phys. **27**, L325 (1994)
- [7] Dehai Bao , Shi-Gang Chen and Jie Liu, Applied Phys. B **62** , 313 (1996)
- [8] L.D.Laudau, and E.M.Lifshitz, 'Quantum Mechanics', P293 (1977) , Pergamon Press
- [9] M.V.Ammosov, N.B.Delone and V.P.Krainov, Zh.Eksp.Teor.Fiz., **91**, (1986), 2008
- [10] Shi-Gang Chen, Jie Liu et al, 'Photoionization and Residual Energy in Ultrashort Pulse Laser', 'Soft X-Ray Lasers and Applications', SPIE, Vol.2520, P113, 1995
- [11] K.C.Kulander, K.J.Schafer and J.L.Krause , 'Dynamics of Short-Pulse Excitation, Ionization and Harmonic Conversion', in 'Super-Intense Laser Laser-Atom Physics', P.95, Ed. Bernard Piraux, Anne L'Huillier and Kazimierz Rzazeewski, Plenum Press, New York, (1993)
- [12] J.G.Leopold and I.C.Percival, J.Phys.B : At.Mol.Opt.Phys. 12, (1979) 709
- [13] Jie Liu and Shi-Gang Chen, Acta Physica Sinica (oversea edition), **4**, 1995, 12
- [14] Edward Ott, 'Chaos in Dynamical System', Cambridge Univ. Press, P.98-99, (1993)
- [15] G.M.Zaslavsky, R.Z.Sadiev, D.A.Usikov and A.A.Chernikov, 'Weak chaos and quasi-regular pattern', P.39, Cambridge Univ. Press, (1991)
- [16] Anne L'Huillier, et al, 'High-Order Harmonic Generation in Rare Gases' in 'Atoms in Intense Laser Fields', P.139, Ed. M.Gavrila, Academic Press, INC. (1992)
- [17] Shih-I Chu, Kwanghsin Wang, and Eric Layton, J.Opt.Soc.Am.B. **7**, (1990), 425
- [18] B.Gunadya, M.Alfred and J.Cooper, Phy.Rev.A.,**41**, (1990), 1744
- [19] K.J.Schafer, B.Yang, L.F.Mauro , and K.C.Kulander, Phys.Rev.Lett., **70**, (1993), 1599, and references there in
- [20] Thomas S.Parker and Leon O.Chua, 'Practical Numerical Algorithms for Chaotic Systems', P.47-54, Springer-Verlag, (1992)
- [21] James F.Heagy, Zi-Min Lu, Jian-Min Yuan, and Michel Vallieres , 'Dynamics of Driven Molecular Systems', in 'Quantum Non-Integrability' , P.322, Ed Da Hsuan Feng and Jian-Min Yuan, World Scientific Publishing, Singapore (1992)
- [22] H.Friedrich and D.Wintgen, Phys.Rep. **183**, 37 (1989)
- [23] G.Casati, B.V.Chirikov, D.L.Shevelyansky, and I.Guarneri, Phys.Rep. **154**, 78 (1987)
- [24] B.Sundaram, R.V.Jensen, Phys.Rev.A **47**, 1415 (1993)
- [25] F.Benvenuto, G.Casati, and D.L.Shevelyansky, Phys.Rev.A, **47**, R786, (1993)
- [26] S.Cocke and L.E.Reichl, Phys.Rev.A **53**, 1746 (1996)
- [27] D.Richards and T.Szeredi, J.Phys.B:At.Mol.Opt.Phys. **28** (1995) L413
- [28] T.Brabec, M.Y.Ivanov, and P.B.Corkum, Phys.Rev.A **54**, R2551 (1996)